Full finite element models and reduction strategies for the simulation of friction-induced vibrations of rolling contact systems

Van-Vuong Lai, Olivier Chiello, Jean-François Brunel, Philippe Dufrenoy

Full finite element models and reduction strategies for the simulation of friction-induced vibrations of rolling contact systems

Van-Vuong Lai[a,b], Olivier Chiello[a,*], Jean-François Brunel[b], Philippe Dufrénoy[b]

[a] *Univ Lyon, IFSTTAR, CEREMA, UMRAE, F-69675, Lyon, France*
[b] *Univ. Lille, CNRS, Centrale Lille, FRE 2016 - LaMcube - Laboratoire de Mécanique Multiphysique Multiéchelle, F-59000, Lille, France*

Abstract

The aim of this paper is to develop a full Finite Element (FE) computational method for the dynamics of unstable frictional rolling contact systems in order to calculate reference solutions in many applications, especially curve squeal for railway transportation but also roller bearing or metal cutting. The proposed method is characterized by the use of a fine FE discretization of the contact surface in an Eulerian frame, nonlinear frictional contact laws and model reduction techniques. An application to the frictional rolling contact between two annular cylinders is presented in both quasi-static and dynamic cases with mode coupling instabilities. The validation of the approach in quasi-static conditions is carried out by comparison with CONTACT software. Stability and transient results show that the technique is able to simulate friction-induced vibrations at high frequencies. Reduced models are tested and show a good agreement with the full model.

Keywords: Curve squeal, Friction-induced vibrations, Rolling contact, Finite element method, Structural instability, Mode coupling, Railway noise.

1. Introduction

A large variety of mechanical system (road vehicle tyres, railway wheels and roller ball bearings, gear box, belt/pulley, lead-screw drives, metal cutting, etc.) generates rolling contact forces which are transferred within a finite area of contact between the rolling element and the substrate. The main reason to make use of rolling contacts in different applications is the low resistance to motion. Even if friction mechanisms are rather weak, they may be an important source of vibration and noise.

As an example in the railway field, the squeal noise emitting by rail-bound vehicles in tight curves (radius lower than 200m) is characterized by high sound pressure levels (130 dB at 0.9m from the wheel) at pure medium and high frequencies. In urban areas where tight curves are numerous, squeal may affect many passengers and local residents and it is necessary to reduce this noise. The modeling of curve squeal can contribute towards an understanding of the generation mechanism and the effects of the different kinematic and mechanical parameters. State of the art brings many models able to simulate curve squeal, distinguished according to mechanisms leading to squeal, wheel/rail contact models and solution domains (time or frequency).

Although longitudinal wheel slip and wheel flange contact have originally been cited as a cause of curve squeal, they have been discredited as a main energy input in several works [1–3]. Most of mechanisms proposed in literature put forward the high lateral slip of the wheel on the rail-head as the main cause of curve squeal. Indeed,

*Corresponding author
Email address: olivier.chiello@ifsttar.fr (Olivier Chiello)

in tight curves, a steady lateral sliding motion is imposed to the wheel due to the misalignment between wheel and rail (angle of attack or yaw angle). A widespread assumption is that the friction forces generated by the sliding motion may lead to structural instability and self-sustained vibration of the wheel/rail system. Two instability mechanisms have been proposed: falling friction and mode coupling. The falling friction was first mentioned by Rudd [1]. A falling slope in the velocity-dependent friction law can be mathematically expressed as negative damping leading to an unstable behavior. A large number of squeal models are based on this mechanism, as in the former paper of Rudd [1] or the more recent works of Heckl *et al.* [4, 5] which explain in detail the mechanism by using frequency-domain and time-domain models. The consideration of mode coupling instability in curve squeal models is more recent. Although such a mechanism may occur with a constant friction coefficient, it needs to take into account the vertical dynamics of the wheel/rail system in order to work. Mathematically, this is the non-symmetric stiffness matrix due to friction which generates the instability. Models proposed in [6–8] consider the mode-coupling mechanism whereas models proposed in [9, 10] considers both falling friction and mode coupling.

For the modeling of rolling contact, there are mainly three kinds of model: point contact models, Kalker's type models with discretized contact surface and finite element models. Extensive reviews can be found for instance in [11, 12]. The first two types have been developed in the context of wheel/rail contact and have been investigated in detail by Kalker using special algorithms and formulations based on linear elasticity. Equivalent point-contact models are based on analytic formulas or heuristic laws of frictional rolling contact such as Hertz theory [13] for the normal problem and Kalker's linear theory [14], Vermeulen and Johnson's model [15], Shen *et al.* model [16] or CHOPAYA law proposed by Ayasse *et al.* [17] for the tangential problem. They are used in quasi-static computations with smooth surfaces, even in the case of large slips. In slightly nonlinear dynamic cases, close to pure rolling, equivalent point stiffness and damping can also be used and give good results, especially for wheel/rail rolling noise modeling [18]. In other cases, including large slips and high-frequency dynamics, surface contact models are more adapted. They need a discretization of the contact zone. Kalker's simplified theory [19] implemented in the algorithm FASTSIM and Kalker's variational theory [14] implemented in CONTACT software are the most used models but other methods exist (cf. for instance Pieringer's model [7]) with slightly different assumptions or resolution techniques. However, some simplifications are generally performed in these models especially in the semi-analytical computation of the local contact flexibilities or influence functions (Boussinesq and Cerruti elastic half-space assumptions, contact/friction decoupling). The impact of these simplifications is rather unknown in the case of friction-induced vibrations characterized by large slips, high frequency dynamics and very fast evolutions at the contact zone. The alternative is to use finite element models. It makes it possible to consider also large deformations and plastic behaviors. The modeling of contact and friction by the finite element method is an active search field. Several variational formulations, discretization methods and specific non linear algorithms exist in the literature [11]. Lagrange multipliers or penalty methods are the most used techniques in order to take into account the constraints corresponding to contact and friction. Dynamics problems require special care since unilateral contact can lead to non-smooth behaviors like localized impacts between the structures [20–22]. In the case of rolling contact, it can be useful not to apply a Lagrangian description but to use a rotating reference frame, notably in order to optimize the meshes of the structures. Finite element treatment based on pure Eulerian or Alternate Lagrangian Eulerian (ALE) formulations for rolling contact problems can be found in [11, 12]. Most applications are quasi-static but such formulations could be advantageously used in high-frequency

dynamics cases. Works dealing with wheel/rail contact analysis by FE methods are quite recent. Bogdansky *et al.* [23] solved the normal problem of static elastic wheel/rail contact in three dimensions with the FE method. The normal problem of contact of elastic-plastic material was investigated by Wiest *et al.* with a 3D static FE model [24]. Other solutions of the normal problem with FE can be found but the treatment of the tangential problem of wheel/rail rolling contact with FE is not frequent. Interesting results are given in the study of Toumi [25] as well as the work of Zhao and Li [26] who treated wheel/rail rolling contact with an explicit FE method. By approaching a quasi-static state, the FE model is notably validated against Hertz theory and CONTACT in both normal and tangential solutions, for the case of wheel treadrail head contact. In these studies, dynamics and contact equations are solved in a Lagrangian frame. All the potential contact area in the rolling direction needs to be meshed with elements of sufficient small size to insure the desired precision. In addition, the meshes of the two potential contact surfaces are not compatible. As a consequence, the treatment of the contact is not straightforward. For instance, Wiest [24] and Toumi [25] used a commercial software where contact between the two bodies is defined using a "masterslave" algorithm. Two types of contact discretization (node-to-surface and surface-to-surface) are used and the results differ depending on the user choice. Efficient algorithms exist for both formulations but, in any case, nonlinear transient FE simulations with frictional contact still remain very expensive in terms of CPU time and memory size when Lagrangian reference frame are considered.

Existing studies can also be distinguished according to the type of researched solutions. Two possible approaches can be used: complex eigenvalue analysis (CEA) and time-integration analysis. On the one hand, stability analyses look for solutions of the linearized dynamic equations governing the system [5, 27–30]. By solving a complex eigenvalue problem or by using the Nyquist criterion, they allow to determine the potential unstable modes and corresponding frequencies of the wheel/rail system and are useful to test the influence of the parameters on the onset of squeal. On the other hand, the dynamic nonlinearities related to the contact evolution at the frictional interfaces can be taken into account using time integration methods and the steady-state amplitudes as well as the full spectrum of squeal can be determined [4, 6, 7, 31–35]. As mentioned by many authors (cf. [36] for instance), both approaches are needed. Indeed, the complex eigenvalue problem may overestimate or underestimate the number of unstable modes. The time integration method can also lead to the appearance of new frequency peaks related to harmonics of the fundamental frequencies of unstable modes. Finally, frequencies of the unstable modes could be different from those resulting from the time integration.

The aim of this paper is to develop a full Finite Element (FE) computational method for the dynamics of frictional rolling contact systems in order to calculate reference solutions of complex systems, for curve squeal noise for example. Continuous equations of the problem are derived around the stationary position of rolling in an Eulerian reference frame. Local unilateral contact and Coulomb friction laws apply on the rolling interface. Weak formulation and FE discretization lead to a nonlinear discrete system which is solved in the time domain by a numerical integration and a point-fixed algorithm at each time step. In addition to the transient approach, a stability analysis performed around the sliding equilibrium position allows to determine unstable modes and frequencies. In order to obtain reasonable computation times, two reduction strategies are proposed. An application of the method to the frictional rolling contact between two annular cylinders is presented in both quasi-static and dynamic cases with mode coupling instabilities.The validation of the approach in quasi-static conditions is carried out by comparison with CONTACT software. Reduction strategies are validated by comparison with the full method.

The main contribution of the paper lies in the whole strategy proposed in order to efficiently compute dynamic transient solutions of rolling/sliding contact systems at high frequencies using finite elements. This strategy is based on the combination of existing techniques: an Eulerian reference frame, numerical tools adapted to the treatment of non-smooth frictional contact laws and reduction methods. The general features of the rolling contact formulations, the non-smooth contact formulations and the reduction methods are not new as part of the finite element method. However, their application to 3D high frequency dynamics of rolling systems with friction is less frequent, essentially due to the computational practical challenge of combining rolling phenomena, nonlinear frictional contact and time integration schemes. The paper provides some tools, which can help the community to compute numerical solutions for this kind of problem, especially in the case of friction-induced vibrations.

2. Finite Element (FE) formulation in the time-domain

2.1. Contact problem in the Eulerian frame

Two bodies in rolling contact are considered, as shown in Fig. 1. The conventions frequently used of rolling contact problems are adopted (cf. for instance [37]). The $z-$axis is chosen to coincide with the common normal to the two surfaces in contact, the longitudinal $x-$axis corresponds to the rolling direction and the $y-$axis refers to the lateral direction. The whole structure is decomposed into two subdomains $\Omega = \Omega_1 \cup \Omega_2$ where subscripts 1 and 2 stand for the upper and the lower bodies respectively. In the absence of deformation and sliding, material particles of each surface move through the contact region in a direction parallel to $x-$axis with rolling speed V. In case of sliding, relative lateral velocities $\Delta V_y = V_{y1} - V_{y2}$ and longitudinal velocities $\Delta V_x = V_{x1} - V_{x2}$ have to be considered. The bodies may also have a relative angular velocity $\Delta\omega_z = \omega_{z1} - \omega_{z2}$ around their common normal (or spin).

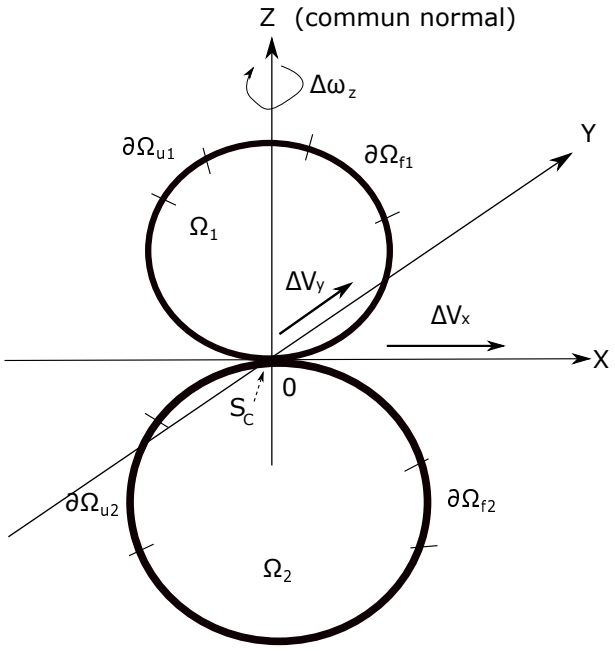

Figure 1: Two bodies in rolling contact

According to [37], in the Eulerian frame which moves with the point of contact, the relative sliding instantaneous velocities (or creep velocities) between the two deformable bodies at a fixed point of the potential contact

interface S_c are given by:

$$\begin{aligned}\dot{s}_x &= v_{x1} - v_{x2} = \Delta V_x - \Delta\omega_z y + V\left(\frac{\partial u_{x1}}{\partial x} - \frac{\partial u_{x2}}{\partial x}\right) + (\dot{u}_{x1} - \dot{u}_{x2}) \\ \dot{s}_y &= v_{y1} - v_{y2} = \Delta V_y + \Delta\omega_z x + V\left(\frac{\partial u_{y1}}{\partial x} - \frac{\partial u_{y2}}{\partial x}\right) + (\dot{u}_{y1} - \dot{u}_{y2})\end{aligned} \tag{1}$$

where $\mathbf{u}(x, y, z, t)$ and $\mathbf{v}(x, y, z, t)$ denote respectively the displacement and velocity fields of the structure in the Eulerian frame, subscripts x and y stand for the spatial components of the fields and the notation $\dot{u} = \frac{\partial u}{\partial t}$ refers to the time partial derivative. The terms involving $V\frac{\partial u}{\partial x}$ represent the deformation contributions due to rolling in the Eulerian frame whereas the terms involving $\dot{u}$ simply represent the dynamic contributions.

In addition, a displacement $\mathbf{u_d}$ is prescribed on the part of the boundary of the domain $\delta\Omega_u = \delta\Omega_{u1} \cup \delta\Omega_{u2}$ and a surface load $\mathbf{f_s}$ is applied on the part $\delta\Omega_f = \delta\Omega_{f1} \cup \delta\Omega_{f2}$. In Ω, a volume load $\mathbf{f_d}$ can be also considered.

2.2. Contact laws

To deal with unilateral contact on the interface, a non-regularized Signorini law is chosen:

$$\begin{aligned}\Delta u_n - g &\leq 0 \\ r_n &\leq 0 \\ (\Delta u_n - g) r_n &= 0\end{aligned} \tag{2}$$

where $\Delta u_n = u_{n1} - u_{n2}$ is the normal relative displacement on the potential contact interface, r_n is the normal contact stress and g is the initial gap. This law simply conveys that (i) there is no interpenetration between the two bodies, (ii) the interface only undergoes compression and (iii) it respects the condition of complementarity. A equivalent semi-regularized form of the law uses the projection on the negative real set (cf. for instance [38]):

$$r_n = \mathrm{Proj}_{\mathbb{R}^-}(r_n - \rho_n \Delta u_n) \qquad \forall \rho_n > 0 \tag{3}$$

where $\mathrm{Proj}_{\mathbb{R}^-}(x) = \min(x, 0)$ and ρ_n is a positive real number called normal augmentation parameter.

To deal with frictional contact, a non-regularized Coulomb law with a constant friction coefficient μ is used:

$$\begin{aligned}\|\mathbf{r}_t\| &\leq -\mu r_n \\ \|\mathbf{r}_t\| = -\mu r_n &\Rightarrow \exists \lambda > 0,\ \dot{\mathbf{s}}_\mathbf{t} = -\lambda \mathbf{r}_t \\ \|\mathbf{r}_t\| < -\mu r_n &\Rightarrow \dot{\mathbf{s}}_\mathbf{t} = 0\end{aligned} \tag{4}$$

where $\dot{\mathbf{s}}_\mathbf{t}$ is the vectorial creep velocity with components $\dot{s}_x$ and $\dot{s}_y$ defined in equation (1) and $\mathbf{r}_t$ is the tangential stress due to friction. This law states that the frictional reaction cannot be greater than a limit $-\mu r_n$. If it reaches the limit, the material particle slides and has a direction opposed to the direction of the reaction (slip state). In other cases, the relative velocity is null (stick state).

A equivalent semi-regularized form of the law uses the projection on the Coulomb cone (cf. for instance [38]):

$$\mathbf{r}_t = \mathrm{Proj}_C(\mathbf{r}_t - \rho_t \dot{\mathbf{s}}_\mathbf{t}) \qquad \forall \rho_t > 0 \tag{5}$$

where $\mathrm{Proj}_C(\mathbf{x}) = \min(\frac{\mu|r_n|}{\|\mathbf{x}\|}, 1)\mathbf{x}$ and ρ_t is a positive real number called tangential augmentation parameter.

2.3. Dynamics equations and FE discretization

A major consequence of the Eulerian frame is to induce convective terms in the equations of motion. These terms are only significant in the case where the rotational speed is in the order of magnitude of the eigenfrequencies ([39]). It is assumed that it is not the case in the present application and the effects of the convective terms are neglected in the following developments.

The displacement field $\mathbf{u}$ must verify the equations of continuum mechanics [40] together with the local formulations of contact equations Eqs. (3) and (5). In order to introduce FE approximations, the principle of virtual power is used for the system dynamics and the contact laws are written in weak forms [41]:

$$\begin{gathered}
\text{find } \mathbf{u} \in \mathcal{U} \text{ and } \mathbf{r} \text{ such as } \forall \mathbf{u}^* \in \mathcal{U}^o \text{ and } \forall \mathbf{r}^* \\
\int_\Omega \rho \mathbf{u}^*.\ddot{\mathbf{u}}\,\mathrm{d}\Omega + \int_\Omega \epsilon(\mathbf{u}^*) : \sigma(\mathbf{u})\,\mathrm{d}\Omega = \int_\Omega \mathbf{u}^*.\mathbf{f}_s\,\mathrm{d}\Omega + \int_{\partial\Omega_F} \mathbf{u}^*.\mathbf{f}_d\,\mathrm{d}s + \int_{S_c} \mathbf{u}^*.\mathbf{r}\,\mathrm{d}s \\
\int_{S_c} r_n^* r_n\,\mathrm{d}s = \int_{S_c} r_n^* \mathrm{Proj}_{\mathbb{R}^-}\left(r_n - \rho_n \Delta u_n\right)\mathrm{d}s \\
\int_{S_c} \mathbf{r}_t^* \mathbf{r}_t\,\mathrm{d}s = \int_{S_c} \mathbf{r}_t^* \mathrm{Proj}_C\left(\mathbf{r}_t - \rho_t \dot{\mathbf{s}}_\mathbf{t}\right)\mathrm{d}s
\end{gathered} \tag{6}$$

where $\epsilon(\mathbf{u})$ and $\sigma(\mathbf{u})$ stand respectively for the symetric gradient and the stress tensor corresponding to any displacement field $\mathbf{u}$, the notation $\ddot{\mathbf{u}} = \frac{\partial^2 \mathbf{u}}{\partial t^2}$ refers to the double time partial derivative, $\mathcal{U} = \{\mathbf{u} | \mathbf{u} = \mathbf{u}_d \text{ on } \partial\Omega_u\}$ and $\mathcal{U}^0 = \{\mathbf{u} | \mathbf{u} = \mathbf{0} \text{ on } \partial\Omega_u\}$.

By using appropriate shape interpolation functions for unknown and test displacement and reaction fields $(\mathbf{u}, \mathbf{r}, \mathbf{u}^*, \mathbf{r}^*)$, finite element discretization of Eq. (6) directly gives:

$$\begin{aligned}
\mathbf{M}\ddot{\mathbf{U}} + \mathbf{C}\dot{\mathbf{U}} + \mathbf{K}\mathbf{U} &= \mathbf{F} + {\mathbf{P_n}}^{\mathrm{T}}\mathbf{R_n} + {\mathbf{P_t}}^{\mathrm{T}}\mathbf{R_t} \\
\mathbf{R_n} &= \int_{S_c} {\mathbf{N_n}}^{\mathrm{T}} \mathrm{Proj}_{\mathbb{R}^-}\left(\mathbf{N_n}\left(\mathbf{H_n^{-1}}\mathbf{R_n} - \rho_n(\mathbf{P_n}\mathbf{U} - \mathbf{G})\right)\right)\mathrm{d}s \\
\mathbf{R_t} &= \int_{S_c} {\mathbf{N_t}}^{\mathrm{T}} \mathrm{Proj}_C\left(\mathbf{N_t}\left(\mathbf{H_t^{-1}}\mathbf{R_t} - \rho_t \dot{\mathbf{S}}_\mathbf{t}(\mathbf{P_t}\mathbf{U}, \mathbf{P_t}\dot{\mathbf{U}})\right)\right)\mathrm{d}s
\end{aligned} \tag{7}$$

where $\mathbf{U}$, $\mathbf{R_n}$ and $\mathbf{R_t}$ denote respectively the vectors of nodal displacements, equivalent normal reactions and equivalent friction forces, $\mathbf{M}, \mathbf{C}, \mathbf{K}$ are respectively the mass, damping and stiffness matrices of the structure without contact, $\mathbf{G}$ is the vector of nodal initial gaps and $\mathbf{N_n}, \mathbf{N_t}$ are the shape function vectors on the contact interface. In addition, $\mathbf{P_n}, \mathbf{P_n}$ are matrices allowing to pass the contact reactions from the local relative frame to the global frame whereas $\mathbf{H_n} = \int_{S_c} {\mathbf{N_n}}^{\mathrm{T}}\mathbf{N_n}\,\mathrm{d}s$ and $\mathbf{H_t} = \int_{S_c} {\mathbf{N_t}}^{\mathrm{T}}\mathbf{N_t}\,\mathrm{d}s$ are transformation matrices from nodal to equivalent forces. Finally, $\dot{\mathbf{S}}_\mathbf{t}(\mathbf{P_t}\mathbf{U}, \mathbf{P_t}\dot{\mathbf{U}})$ denotes the vector of nodal creep velocities which can be determined linearly from local displacement and velocity vectors, taking into account quasi-static creep velocities (cf. Eq. (1)).

3. Reduction strategies

As the size of the system is often large and the nonlinear solving process implies several resolutions of a linear system at each time step, reducing the size of the system is necessary to obtain reasonable computation times. The principle is to search an approximated solution $\mathbf{U} = \mathbf{B}\mathbf{q_r}$ of the problem spanned by a reduced basis $\mathbf{B}$ which leads to a reduced dynamics equation:

$$\mathbf{M_r}\ddot{\mathbf{q}}_\mathbf{r} + \mathbf{C_r}\dot{\mathbf{q}}_\mathbf{r} + \mathbf{K_r}\mathbf{q_r} = \mathbf{B}^{\mathrm{T}}(\mathbf{F} + {\mathbf{P_n}}^{\mathrm{T}}\mathbf{R_n} + {\mathbf{P_t}}^{\mathrm{T}}\mathbf{R_t}) \tag{8}$$

where $\mathbf{M_r}, \mathbf{C_r}, \mathbf{K_r} = \mathbf{B}^{\mathrm{T}}(\mathbf{M_r}, \mathbf{C_r}, \mathbf{K_r})\mathbf{B}$ and the size of the system is reduced to the number of modes in basis $\mathbf{B}$.

In the field of friction-induced vibrations, the use of *a priori* reduction bases remains a commonly used technique for industrial systems but the performance of the bases depends on the application. In the case of a simplified brake squeal application, Brizard *et al.* proposed several optimized reduction bases for the stability analysis [42]. For the same application, Lorang and Chiello [43] showed a strong participation of the unstable complex mode shapes determined by the stability analysis in the nonlinear solution, suggesting that reduction bases based on unstable complex modes could be used in the nonlinear problem. However, Sinou [36] observed that the contributions of the harmonic components and the combination of frequency components can not be neglected. Loyer *et al.* [22] performed intensive simulations in order to test two types of bases. The degrees of freedom at contact interface are kept in these bases based on the complex modes resulting from the stability analysis. The study notably shows that an accurate model reduction for friction-destabilized system is possible but requires great care. In particular, all the stable modes in the frequency range must be included to ensure an accurate prediction of the nonlinear response. In addition, if separation at the interface is present, the reduction basis must also contain corresponding static boundary modes.

It should also be noted that some other performant techniques exist for the reduction of non linear dynamic systems. To determine relevant reduction bases, it is thus possible to use singular value decomposition (SVD) of Proper Orthogonal Decomposition [44] of some representative sets of the full temporal solution to extract the major shapes. The concept of nonlinear modes [45] was also developed in recent years and proves to be efficient in some applications. For autonomous systems with mono-instabilities (only one unstable mode), the benefit is small since the searched periodic limit cycles are precisely the nonlinear modes.

In this paper, the proposed basis is rather classical and is based on an *a priori* selection of free-interface normal modes enriched by static local modes.

3.1. Component Mode Synthesis (CMS) with free-interface modes

A first reduction basis includes free-interface normal modes of the structure and static attachment modes $\mathbf{B} = [\mathbf{\Phi} \quad \mathbf{\Phi}_s]$. Matrix $\mathbf{\Phi}$ contains the real solutions of the free and undamped system:

$$(\mathbf{K} - \omega^2\mathbf{M})\mathbf{U} = \mathbf{0} \tag{9}$$

whereas $\mathbf{\Phi}_s$ make the base statically complete by adding static solutions to unitary forces (normal and tangential) on the contact interface:

$$\mathbf{K}\mathbf{\Phi}_s = \mathbf{P_c}^{\mathrm{T}} \tag{10}$$

where $\mathbf{P_c}^{\mathrm{T}} = [\mathbf{P_n}^{\mathrm{T}} \quad \mathbf{P_t}^{\mathrm{T}}]$. In order to improve the numerical efficiency, the basis is then orthogonalized in relation to stiffness matrix $\mathbf{K}$ before use. It is well-known that static attachment modes are useful to provide a better approximation of the dynamics by comparison with normal modes alone. It is also worth noticing that the size of the basis is $n_m + 3n_c$ where n_m is the number of normal modes taken into account in the frequency range of interest and n_c is the number of facing nodes on the interface.

3.2. Contact static approximation

A stronger approximation consists in neglecting the dynamic terms in the reduced equations corresponding to attachment modes. However, bases $\mathbf{\Phi}$ and $\mathbf{\Phi}_s$ are not orthogonal which is a necessary condition in order to separate

the contributions of normal modes and attachment modes. This can be fixed by using residual attachment modes defined by:

$$\tilde{\mathbf{\Phi}}_s = \mathbf{\Phi}_s - \mathbf{\Phi}(\mathbf{\Phi}^{\mathrm{T}}\mathbf{K}\mathbf{\Phi})^{-1}\mathbf{\Phi}^{\mathrm{T}}{\mathbf{P_c}}^{\mathrm{T}} \tag{11}$$

These modes are the static displacement responses to unit contact reactions after the elimination of the contribution of normal modes. It can be easily verified that $\tilde{\mathbf{\Phi}}_s^{\mathrm{T}}\mathbf{K}\mathbf{\Phi} = \mathbf{0}$.

The use of basis $\mathbf{B} = [\mathbf{\Phi} \quad \tilde{\mathbf{\Phi}}_s]$ in Eq. (8) together with the elimination of the dynamic terms relating to attachment modes gives:

$$\begin{aligned} \mathbf{\Phi}^{\mathrm{T}}\mathbf{M}\mathbf{\Phi}\ddot{\mathbf{q}} + \mathbf{\Phi}^{\mathrm{T}}\mathbf{C}\mathbf{\Phi}\dot{\mathbf{q}} + \mathbf{\Phi}^{\mathrm{T}}\mathbf{K}\mathbf{\Phi}\mathbf{q} &= \mathbf{\Phi}^{\mathrm{T}}(\mathbf{F} + {\mathbf{P_n}}^{\mathrm{T}}\mathbf{R_n} + {\mathbf{P_t}}^{\mathrm{T}}\mathbf{R_t}) \\ \tilde{\mathbf{\Phi}}_s^{\mathrm{T}}\mathbf{K}\tilde{\mathbf{\Phi}}_s\mathbf{q_s} &= \tilde{\mathbf{\Phi}}_s^{\mathrm{T}}(\mathbf{F} + {\mathbf{P_n}}^{\mathrm{T}}\mathbf{R_n} + {\mathbf{P_t}}^{\mathrm{T}}\mathbf{R_t}) \end{aligned} \tag{12}$$

where $\mathbf{q}$ and $\mathbf{q_s}$ are the generalized coordinate vectors corresponding respectively to normal modes and residual attachment modes such that $\mathbf{U} = \mathbf{\Phi}\mathbf{q} + \tilde{\mathbf{\Phi}}_s\mathbf{q_s}$. A total decoupling between the generalized equations corresponding to free-interface normal modes and residual static attachment modes is obtained.

In addition, noticing that:

$$\begin{aligned} \tilde{\mathbf{\Phi}}_s^{\mathrm{T}}\mathbf{K}\tilde{\mathbf{\Phi}}_s\mathbf{q_s} &= \left(\mathbf{\Phi}_s^{\mathrm{T}} - \mathbf{P_c}\mathbf{\Phi}(\mathbf{\Phi}^{\mathrm{T}}\mathbf{K}\mathbf{\Phi})^{-1}\mathbf{\Phi}^{\mathrm{T}}\right)\mathbf{K}\left(\mathbf{\Phi}_s - \mathbf{\Phi}(\mathbf{\Phi}^{\mathrm{T}}\mathbf{K}\mathbf{\Phi})^{-1}\mathbf{\Phi}^{\mathrm{T}}{\mathbf{P_c}}^{\mathrm{T}}\right)\mathbf{q_s} \\ &= \left(\mathbf{P_c}\mathbf{\Phi}_s - \mathbf{P_c}\mathbf{\Phi}(\mathbf{\Phi}^{\mathrm{T}}\mathbf{K}\mathbf{\Phi})^{-1}\mathbf{\Phi}^{\mathrm{T}}{\mathbf{P_c}}^{\mathrm{T}}\right)\mathbf{q_s} \\ &= \mathbf{P_c}\tilde{\mathbf{\Phi}}_s\mathbf{q_s} \\ &= \mathbf{P_c}(\mathbf{U} - \mathbf{\Phi}\mathbf{q}) \end{aligned} \tag{13}$$

and including the above expression in Eq. (12) gives:

$$\begin{aligned} \mathbf{\Phi}^{\mathrm{T}}\mathbf{M}\mathbf{\Phi}\ddot{\mathbf{q}} + \mathbf{\Phi}^{\mathrm{T}}\mathbf{C}\mathbf{\Phi}\dot{\mathbf{q}} + \mathbf{\Phi}^{\mathrm{T}}\mathbf{K}\mathbf{\Phi}\mathbf{q} &= \mathbf{\Phi}^{\mathrm{T}}(\mathbf{F} + {\mathbf{P_n}}^{\mathrm{T}}\mathbf{R_n} + {\mathbf{P_t}}^{\mathrm{T}}\mathbf{R_t}) \\ \mathbf{P_c}\mathbf{U} &= \tilde{\mathbf{\Phi}}_s^{\mathrm{T}}(\mathbf{F} + {\mathbf{P_n}}^{\mathrm{T}}\mathbf{R_n} + {\mathbf{P_t}}^{\mathrm{T}}\mathbf{R_t}) + \mathbf{P_c}\mathbf{\Phi}\mathbf{q} \end{aligned} \tag{14}$$

It must be emphasized that, with this formulation, contact displacements $\mathbf{P_c}\mathbf{U}$ can be directly calculated from expanded forces and normal modes coordinates.

This reduction strategy consists in solving the global dynamics using free-interface normal modes and adding a local static residual flexibility controlled by matrix $\tilde{\mathbf{\Phi}}_s^{\mathrm{T}}$ in the expression of the contact displacements. This allows to determine the contact displacements with a high precision level which is needed to solve the frictional contact laws and calculate the reaction forces. This method gets very close to models such Pieringer's one [7] combining modal dynamics and static local resolutions of the kind of CONTACT software. However, in the proposed method, the local flexibility is calculated numerically by finite elements instead of using semi-analytical influence functions derived from Boussinesq's approximations. In particular, it takes into account the static normal/tangential coupling at the contact zone. It also depends on the number of free-interface modes in the basis since it corresponds to a residual flexibility.

4. Stability analysis

The aim of the stability analysis is to address the mechanism of self-excited vibration due to frictional contact through the determination of the evolution of small perturbations around the steady sliding equilibrium. In stable cases, the perturbations vanish and no vibration occur. In unstable cases, some perturbations tend to diverge which can lead to self-sustained vibrations. Such an analysis is performed by a linearization of the non-linear equations around the equilibrium.

4.1. Quasi-static equilibrium

The quasi-static or steady sliding equilibrium is first obtained by neglecting the dynamic terms in Eqs. (1) and (7):

$$\begin{aligned}\mathbf{K}\mathbf{U}^{\mathbf{e}} &= \mathbf{F} + \mathbf{P}_{\mathbf{n}}^{\mathrm{T}}\mathbf{R}_{\mathbf{n}}^{\mathbf{e}} + \mathbf{P}_{\mathbf{t}}^{\mathrm{T}}\mathbf{R}_{\mathbf{t}}^{\mathbf{e}} \\ \mathbf{R}_{\mathbf{n}}^{\mathbf{e}} &= \int_{S_c} \mathbf{N}_{\mathbf{n}}^{\mathrm{T}}\mathrm{Proj}_{\mathbb{R}^-}\left(\mathbf{N}_{\mathbf{n}}\left(\mathbf{H}_{\mathbf{n}}^{-\mathbf{1}}\mathbf{R}_{\mathbf{n}}^{\mathbf{e}} - \rho_n(\mathbf{P}_{\mathbf{n}}\mathbf{U}^{\mathbf{e}} - \mathbf{G})\right)\right)\mathrm{d}s \\ \mathbf{R}_{\mathbf{t}}^{\mathbf{e}} &= \int_{S_c} \mathbf{N}_{\mathbf{t}}^{\mathrm{T}}\mathrm{Proj}_{C}\left(\mathbf{N}_{\mathbf{t}}(\mathbf{H}_{\mathbf{t}}^{-\mathbf{1}}\mathbf{R}_{\mathbf{t}} - \rho_t\dot{\mathbf{S}}_{\mathbf{t}}^{\mathbf{e}})\right)\mathrm{d}s\end{aligned} \tag{15}$$

where $\dot{\mathbf{S}}_{\mathbf{t}}^{\mathbf{e}} = \dot{\mathbf{S}}_{\mathbf{t}}(\mathbf{P}_{\mathbf{t}}\mathbf{U}^{\mathbf{e}}, \mathbf{0})$ is the vector of nodal quasi-static creepage velocities.

Assuming that some solutions of Eq. (15) exist and can be calculated, it notably provides the status of the nodes on the contact interface as a function of the equivalent normal reactions r_n^e and friction forces $\mathbf{r}_t^e$:

- if $r_n^e = 0$, the facing nodes are not in contact,
- if $r_n^e \neq 0$ and $\|\mathbf{r}_{\mathbf{t}}^{\mathbf{e}}\| < -\mu r_n^e$ the facing nodes are sticking,
- if $r_n^e \neq 0$ and $\|\mathbf{r}_t^e\| = -\mu r_n^e$ the facing nodes are sliding ; the sliding direction of the friction force is then given by $\mathbf{t} = \mathbf{r}_t^e/\|\mathbf{r}_t^e\|$.

4.2. Complex Eigenvalue Analysis (CEA) in case of full steady sliding

In this paper, stability analysis is only carried out in the case of full steady sliding (no sticking region) and maintained contact configuration: it is thus assumed that for each node in contact at equilibrium, bilateral contact and sliding Coulomb friction laws apply. In order to perform the stability analysis, these laws have to be linearized. On effective contact region, the linearized forms of Eqs. (3) and (5) with the above assumptions can be written (cf. for instance [42]):

$$\begin{aligned}\Delta u_n &= 0 \\ \mathbf{r}_t &= -\mu r_n \mathbf{t} - c_b \dot{u}_b \mathbf{b}\end{aligned} \tag{16}$$

where $c_b = -\mu r_n^e/\|\dot{\mathbf{s}}_t^e\|$ is a damping term due to the linearisation of the sliding direction of the friction force and $\mathbf{b}$ is the tangential direction orthogonal to $\mathbf{t}$.

Searching a discrete solution of the form $\mathbf{U}^{\mathbf{e}} + \tilde{\mathbf{U}}\exp(\lambda t)$ where $\tilde{\mathbf{U}}$ stands for the complex displacement vector corresponding to small harmonic perturbations around the equilibrium, the linearized form of equation (7) leads to a constrained non symmetric eigenvalues problem:

$$\begin{aligned}\left(\lambda^2\mathbf{M} + \lambda(\mathbf{C} + \mathbf{C}_{\mathbf{b}}) + \mathbf{K}\right)\tilde{\mathbf{U}} &= (\tilde{\mathbf{P}}_{\mathbf{n}}^{\mathrm{T}} + \mu\tilde{\mathbf{P}}_{\mathbf{t}}^{\mathrm{T}})\tilde{\mathbf{R}}_{\mathbf{n}} \\ \tilde{\mathbf{P}}_{\mathbf{n}}\tilde{\mathbf{U}} &= 0\end{aligned} \tag{17}$$

where $\mathbf{C}_{\mathbf{b}}$ is the damping matrix provided by the linearisation of the sliding direction of friction force [22, 42, 46] and $\tilde{\mathbf{P}}_{\mathbf{n}}, \tilde{\mathbf{P}}_{\mathbf{t}}$ are new projection matrices such that $\tilde{\mathbf{P}}_{\mathbf{n}}$ is the restriction of $\mathbf{P}_{\mathbf{n}}$ on nodes in the effective contact region at equilibrium whereas $\tilde{\mathbf{P}}_{\mathbf{t}}$ is the restriction of $\mathbf{P}_{\mathbf{t}}$ on components in direction $\mathbf{t}$ on nodes in the effective contact region.

Complex modes and eigenvalues of the problem are then calculated. Modes corresponding to eigenvalues with positive real part are unstable. The divergence rate of a mode is notably defined as $\mathrm{Re}(\lambda)/\mathrm{Im}(\lambda)$ where $(\mathrm{Re}(\lambda), \mathrm{Im}(\lambda))$ are respectively the real and imaginary parts (pulsation) of the mode. This rate corresponds to a negative damping rate.

4.3. Reduced CEA formulations

Solving such a large non-symmetric eigenvalue problem needs model reduction. Several reduction bases have been notably tested by following the methodology proposed by Brizard [42]. The two reduction strategies proposed in the nonlinear case (section 3) are adapted here for the stability analysis.

4.3.1. Component Mode Synthesis with free-interface modes

The first reduced basis includes free-interface normal modes of the structure and static attachment modes $\mathbf{B} = [\mathbf{\Phi} \quad \mathbf{\Phi}_s]$ as proposed in section 3 but defined on effective contact region by using $\tilde{\mathbf{P}}_\mathbf{n}$ and $\tilde{\mathbf{P}}_\mathbf{t}$ instead of $\mathbf{P}_\mathbf{n}$ and $\mathbf{P}_\mathbf{t}$. In order to solve the eigenvalue problem with this reduced basis, the constraints are directly added to the generalized coordinates associated to the modes (cf. [47, 48] for symmetric normal problems and [22, 42] for non-symmetric friction problems).

4.3.2. Contact static approximation

The stronger approximation consisting in neglecting the dynamic part of the attachment modes is also tested for the stability analysis. The same technique used in section 3 is applied. The reduction is first performed with basis $\mathbf{B} = [\mathbf{\Phi} \quad \tilde{\mathbf{\Phi}}_s]$ composed of free-interface component modes $\mathbf{\Phi}$ and static attachment residual modes $\tilde{\mathbf{\Phi}}_s$ defined on effective contact region. The dynamic effects corresponding the residual attachment modes are then neglected leading to the following constrained eigenvalue problem:

$$\begin{aligned}\left(\lambda^2\mathbf{\Phi}^\mathrm{T}\mathbf{M}\mathbf{\Phi} + \lambda\mathbf{\Phi}^\mathrm{T}(\mathbf{C}+\mathbf{C_b})\mathbf{\Phi} + \mathbf{\Phi}^\mathrm{T}\mathbf{K}\mathbf{\Phi}\right)\tilde{\mathbf{q}} &= \mathbf{\Phi}^\mathrm{T}(\tilde{\mathbf{P}}_\mathbf{n}^\mathrm{T} + \mu\tilde{\mathbf{P}}_\mathbf{t}^\mathrm{T})\tilde{\mathbf{R}}_\mathbf{n} \\ \tilde{\mathbf{P}}_\mathbf{c}\tilde{\mathbf{U}} &= \tilde{\mathbf{\Phi}}_s^\mathrm{T}(\tilde{\mathbf{P}}_\mathbf{n}^\mathrm{T} + \mu\tilde{\mathbf{P}}_\mathbf{t}^\mathrm{T})\tilde{\mathbf{R}}_\mathbf{n} + \tilde{\mathbf{P}}_\mathbf{c}\mathbf{\Phi}\tilde{\mathbf{q}} \\ \tilde{\mathbf{P}}_\mathbf{n}\tilde{\mathbf{U}} &= \mathbf{0}\end{aligned} \tag{18}$$

where $\tilde{\mathbf{q}}$ is the generalized vector corresponding to free-interface normal modes.

From the two last lines of Eq. (18), normal reactions $\tilde{\mathbf{R}}_\mathbf{n}$ can be expressed as a function of the generalized vector $\tilde{\mathbf{q}}$:

$$\tilde{\mathbf{R}}_\mathbf{n} = -\left(\mathbf{I}_n\tilde{\mathbf{\Phi}}_s^\mathrm{T}(\tilde{\mathbf{P}}_\mathbf{n}^\mathrm{T} + \mu\tilde{\mathbf{P}}_\mathbf{t}^\mathrm{T})\right)^{-1}\tilde{\mathbf{P}}_\mathbf{c}\mathbf{\Phi}\tilde{\mathbf{q}} \tag{19}$$

where $\mathbf{I}_n$ is the Boolean localization matrix such that $\tilde{\mathbf{P}}_\mathbf{n} = \mathbf{I}_n\tilde{\mathbf{P}}_\mathbf{c}$. Finally, using the above expression in the reduced eigenvalue problem gives:

$$\left(\lambda^2\mathbf{\Phi}^\mathrm{T}\mathbf{M}\mathbf{\Phi} + \lambda\mathbf{\Phi}^\mathrm{T}(\mathbf{C}+\mathbf{C_b})\mathbf{\Phi} + \mathbf{\Phi}^\mathrm{T}(\mathbf{K}+\mathbf{K_c})\mathbf{\Phi}\right)\tilde{\mathbf{q}} = \mathbf{0} \tag{20}$$

where $\mathbf{K_c}$ is a non-symmetric stiffness matrix taking account the effect of the local residual flexibility of the structure due to normal and friction forces:

$$\mathbf{K_c} = (\tilde{\mathbf{P}}_\mathbf{n}^\mathrm{T} + \mu\tilde{\mathbf{P}}_\mathbf{t}^\mathrm{T})\left(\mathbf{I}_n\tilde{\mathbf{\Phi}}_s^\mathrm{T}(\tilde{\mathbf{P}}_\mathbf{n}^\mathrm{T} + \mu\tilde{\mathbf{P}}_\mathbf{t}^\mathrm{T})\right)^{-1}\tilde{\mathbf{P}}_\mathbf{n} \tag{21}$$

This reduction strategy consists in solving the global dynamics using free-interface normal modes and adding a local static residual stiffness controlled by matrix $\mathbf{K_c}$. This matrix plays the same role than 2-DOF Hertzian stiffness/Coulomb friction relations in the case on equivalent point contact models but is calculated by finite elements.

5. Numerical methods for nonlinear simulations

For the determination of quasi-static and transient solutions from Eqs. (7) and (15), with or without reduction, the following numerical methods are used.

5.1. Integration scheme for the dynamics

For the computation of the transient solution, the chosen time integration method is a modified θ-method. This is a first-order scheme developed by Jean [38] and appropriate to unilateral contact dynamics. It notably allows to compute quasi-inelastic shocks. A value $\theta = 0.5$ is chosen to avoid numerical damping. The detail of the scheme with an application to friction-induced vibrations can be found for instance in Loyer's work [22].

5.2. Non-linear resolution

For the computation of the quasi-static solution and dynamics solutions at each time step, an iterative fixed point algorithm on equivalent contact reactions and friction forces is used with a stop criterion based on forces convergence [22]. This algorithm is appropriate to the formulation of the frictional contact laws as nonlinear projections. The main advantage of the fixed point algorithm is that the integrator matrix remains constant at each iteration. In the simulations presented in this paper, the augmented parameters ρ_n, ρ_t are chosen as the smallest eigenvalue of the integrator matrix condensed on the contact degrees of freedom [49]. More optimized parameters can be found in [22] but have not been used.

6. Results

In this section, an application of the methodology presented in the previous sections is proposed for the case of rolling contact of two annular cylinders with lateral creepages. The model is first described. Second, the model is validated in quasi-static conditions with CONTACT software. Considering that there is no reference approach in the dynamic case, this quasi-static validation is essential in order to show that the proposed method is able to accurately reproduce the creep phenomenon characterized by an effective contact area separated in two (stick and slip) zones. A stability analysis is then carried out. Transient calculations are finally performed with and without reduction and results are discussed and compared.

6.1. Description of the model

A rolling contact between two same annular cylinders is considered, as shown in Fig. 2. The material behavior is assumed to be linearly elastic, isotropic and undergoing small deformations. A Rayleigh damping with coefficients α and β is introduced in the model. The values of α and β have been chosen in order to obtain modal damping factors comprised between 0.5 % and 5 % in the frequency range of interest of [100-5000] Hz. These quite high values are useful to show that the found instabilities are strong and do not disappear with any small damping in the structures (cf. section 6.4). The material and geometrical parameters of the cylinders are listed in Tab. 1.

A vertical displacement u_{z0} is applied at the hub of the upper cylinder whereas a rigid constraint is applied at the lower cylinder. For the discretization by finite elements, compatible meshes on the interface are considered: facing nodes of the two cylinders in potential contact have identical tangential coordinates x and y. The global meshes of the cylinders have been chosen in order to respect the dynamic criterion of 10 elements per wavelength for the free normal modes in the frequency range of interest. The meshing of the contact zone have to allow an accurate description of the slip/stick transition in the area. Consequently, the size of the elements in the contact zone have to be much smaller than the dimensions of the effective area (at least an order of magnitude). On the other hand, the

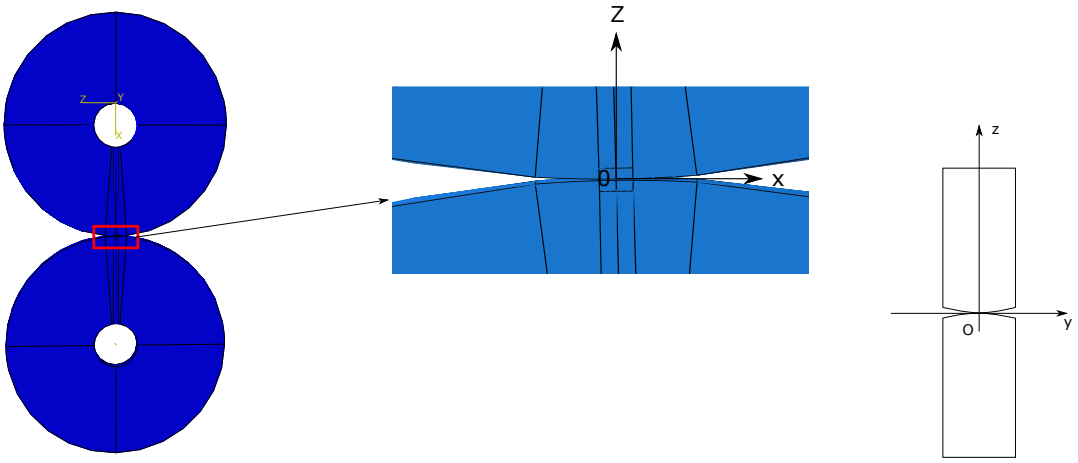

(a) (b)

Figure 2: Contact between two annular cylinders with lateral curvatures and contact point in the center (a:Front view with zoom on the contact zone, b: Side view)

Table 1: Material and geometrical parameters of the cylinders

Young's modulus	205 GPa
Poisson's ratio	0.3
Density	7800 kg/m^3
Rayleigh's damping coefficients (α, β)	$(1, 10^{-6})$
Internal radius	0.1 m
External radius	0.5 m
Thickness	0.05 m

size of the problem can become very large when the number of contact dofs increases. In this application, Hertz theory gives the dimensions of (4.5, 4.5) mm for the contact area. The convergence of the quasi-static and dynamic solutions gives an optimal size of 1 mm for the elements at the contact zone as shown in Fig. 3.

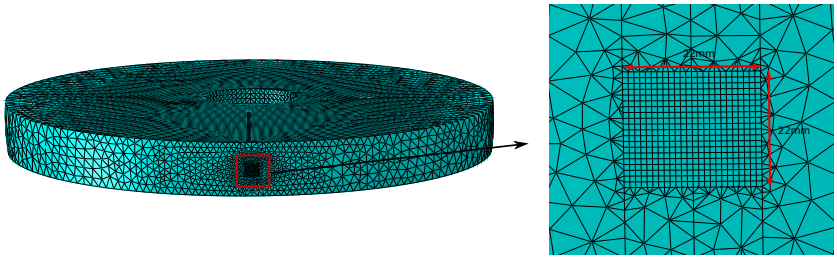

Figure 3: FE model of a cylinder with fine mesh on the contact zone

Actually, in the proposed application, the two cylinders are fully symmetrical and it would have been possible to model only one cylinder using symmetry relations.

6.2. *Free-interface normal modes*

The 80 first natural frequencies and corresponding free-interface modes have been calculated up to 7510 Hz. The eigenmodes are classified according to their predominant deformations (axial, radial or circumferential) and their numbers (n, m) of nodal diameters and nodal circles. Two modes are represented in Fig. 4. This classification is necessary to determine the optimal mesh according to a targeted number of element per wavelength for the free normal modes. However, no convergence study has been performed in order to examine the effect of these meshes on the full model with frictional contact (nor for stability analysis either for self-sustained vibrations).

(a) (b)

Figure 4: Examples of free eigenmodes of a cylinder (a: Axial mode (0,2) (316 Hz), b: Radial mode (0,3)(3695 Hz))

6.3. *Quasi-static results*

In this section the quasi-static rolling contact of the two cylinders with lateral creepage is considered. The contact zone is supposed to be laterally centered. As shown in Fig. 2b, the geometry of the lateral profiles of the two cylinders has been curved in order to obtain an effective 3-dimensional contact. For each cylinder the applied

radius of curvature is 0.5 m. The rolling is performed in the $-x$ direction with $V = 10$ m/s. An vertical displacement $u_{z0} = 0.1$ mm is applied leading to a resultant vertical contact force of about 75 kN. A friction coefficient $\mu = 0.3$ is considered. Longitudinal and spin creepages are set to zero ($\Delta V_x = \Delta\omega_z = 0$).

For an imposed lateral creepage $\Delta V_y/V = 0.3\%$, the longitudinal distributions of the normal contact stresses P_n and frictional stresses P_t on the center line of the contact zone ($y = 0$) are presented in Fig. 5. As expected, a stick zone occurs at the leading edge of the contact and a slip zone occurs at the trailing edge of the contact. The comparison of the results obtained with the proposed full FE method and the results provided by CONTACT software shows a good agreement with some small differences for the tangential stresses in the transition between the stick zone and the slip zone.

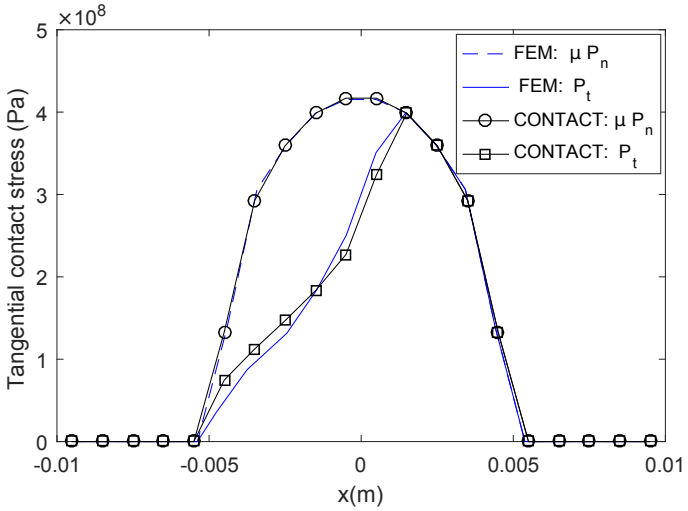

Figure 5: Quasi-static frictional stresses along the line $y = 0$ for $\Delta V_y/V = 0.3\%$ and $\mu = 0.3$

As in the finite element method proposed, Kalker's variational theory [14] implemented in CONTACT software is based on a discretization of the contact zone combined with unilateral contact and Coulomb friction laws. The differences mainly lie in the two simplifications proposed by Kalker in order to calculate the distribution of stresses and deformations in the contact area: local flexibilities computed by using Boussinesq and Cerruti (static) elastic half-space assumptions and decoupling between the normal and tangential problems. Another difference concerns the interpolation functions in the contact zone (linear in the proposed method versus constant in CONTACT software). This can explain the small differences between the results obtained with both methods. As fewer approximations are involved in the proposed method than in Kalker's theory, the results obtained with the finite element method are supposed to be more accurate. However, in such a quasi-static configuration, the differences can simply come from the interpolation functions.

6.4. Stability results

Stability analysis is carried out in case of full sliding using a higher creepage $\Delta V_y/V = 1\%$ by using 160 free-interface normal modes (80 for each cylinder). In order to solve the non symmetric eigenvalue problem, the two reduction strategies presented in section 4.3 (classical CMS and contact static approximation) are tested and compared with reference results obtained with an iterative method minimizing the force residue, like in [42].

In the case where the contact point is centered, no instability is found whatever the friction coefficient. In order to obtain instabilities the contact point is laterally shifted, as shown in Fig. 6. This offset increases the

lateral/vertical coupling which is a necessary condition to obtain mode-coupling instabilities. The lateral position of the contact point seems to be one of the most important parameter for the occurrence of instabilities. Indeed, it bring out a stronger coupling between the normal and tangential dynamics due to the asymmetrical geometry of the system compared with the centered position.

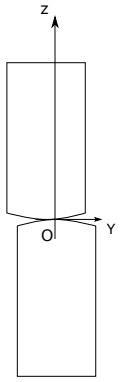

Figure 6: Lateral offset of the contact point

With an lateral offset $u_{y0} = 4$ cm, one mode is founded to be unstable. Results obtained with $\mu = 0.3$ are shown in Fig. 7. The real part of a complex mode at frequency 1609 Hz is positive. The corresponding mode shape is presented in Fig. 8.

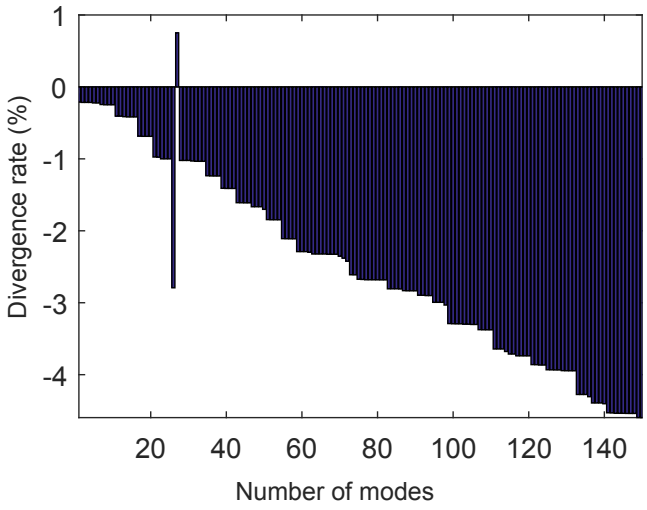

Figure 7: Divergence rate of complex eigenvalues for $\Delta V_y/V = 1\%$ and $\mu = 0.3$

In order to confirm the mode-coupling instability and to test the behavior of the reduced basis presented in section 4.3, the evolution of the eigenvalues corresponding to the two complex modes involved in the instability (i.e. the bifurcation curves) are represented in Fig. 9 without damping (by imposing $\mathbf{C} = \mathbf{C_b} = \mathbf{0}$) and in Fig. 10 with damping. As expected, the increase of the friction coefficient brings the two modes closer until their frequencies coalesce and one mode becomes unstable.

In order to analyze the case with damping, a brief discussion about the known effects of damping on coalescence patterns is needed. Indeed, these effects are not straightforward as shown for instance [20, 50, 51]. In particular, a non-uniform repartition of damping between the modes involved in the coalescence can destabilize the system in some cases, especially trough a smoothing effect. In the present system, the internal viscous damping

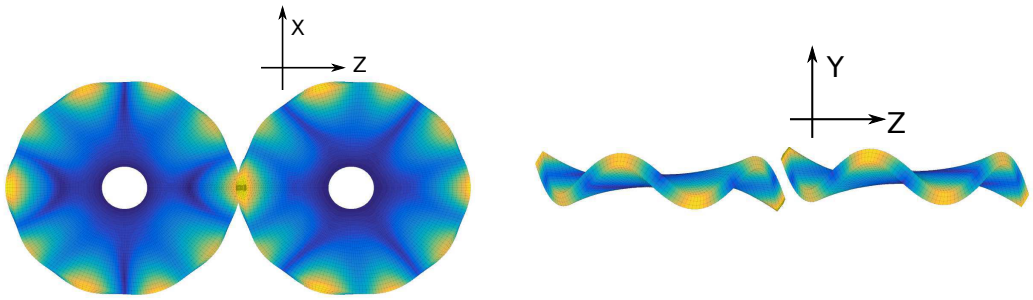

Figure 8: Unstable mode for $\Delta V_y/V = 1\%$ and $\mu = 0.3$

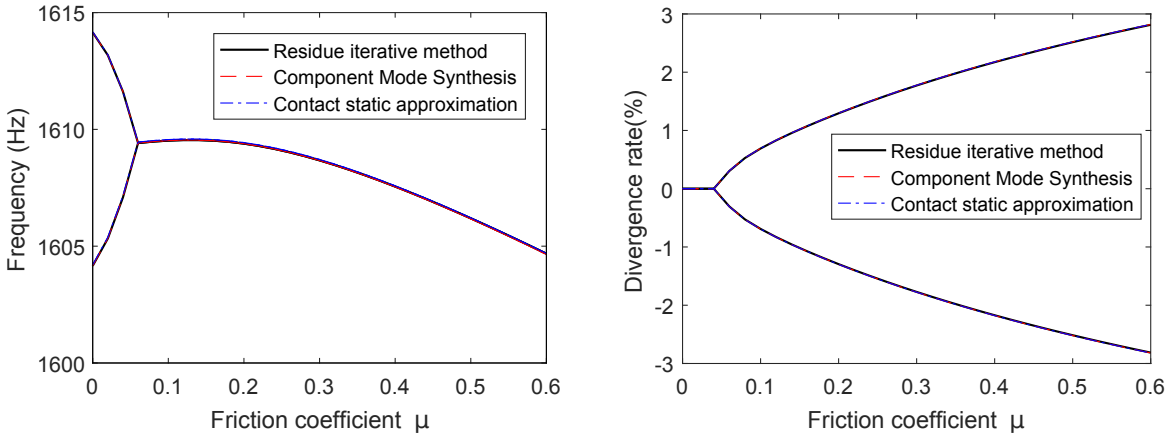

(a) (b)

Figure 9: Evolutions of the frequency and divergence rate of complex modes without damping for $\Delta V_y/V = 1\%$ (a: Frequency, b: Divergence rate)

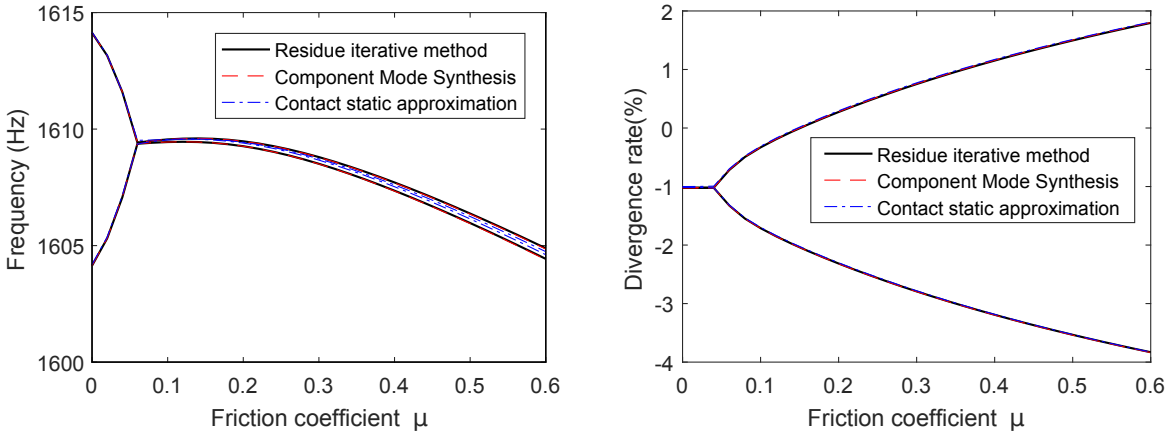

(a) (b)

Figure 10: Evolutions of the frequency and divergence rate of complex modes with damping for $\Delta V_y/V = 1\%$ (a: Frequency, b: Divergence rate)

in the structures is proportional and the two modes involved in the instability are equally damped at $\mu = 0$. Thus, in this special case, only a lowering effect is expected, which tends to stabilize the mechanical system by shifting vertically the bifurcation curves in comparison with the undamped case. This can be observed in Fig. 10b. To be rigorous, it should be noted that the linearization of the planar friction force in Eq. (16) leads to an added damping effect (matrix $\mathbf{C_b}$), which is nor proportional either equally distributed between the modes or could be a smoothing factor as show in [21]. However, in the present application, this effect seems to be negligible compared to the high internal damping. Concerning the evolution of the frequencies in Fig. 10a, the results also comply with previous observations, showing a dispersion of the curves after the merging point.

With regard to reduction strategies, the first validation has been performed by comparing the real and imaginary parts of complex pulsations provided by the different bases in the CEA for the reference friction coefficient $\mu = 0.3$. As recommended in Brizard's work, the highest frequency of the modes taken into account has to be equal to 1.5 times the upper frequency of the frequency range of interest, i.e. 7546 Hz. The number of free normal modes in the CMS and CSA bases are chosen with this criterion. Thus, 80 free normal modes per disc have been retained, i.e. 160 modes in all. To go further, the validation has been done for $\mu = 0$ to 0.6 but only for the complex pulsations of the two modes involved in the instability (bifurcation curves). The relative errors on the frequencies and the absolute errors on the divergence rates of complex modes obtained with the two proposed reduction bases in comparison with the results obtained with the iterative method are presented in Figs. 11 and 12. It is observed that the differences are very small.

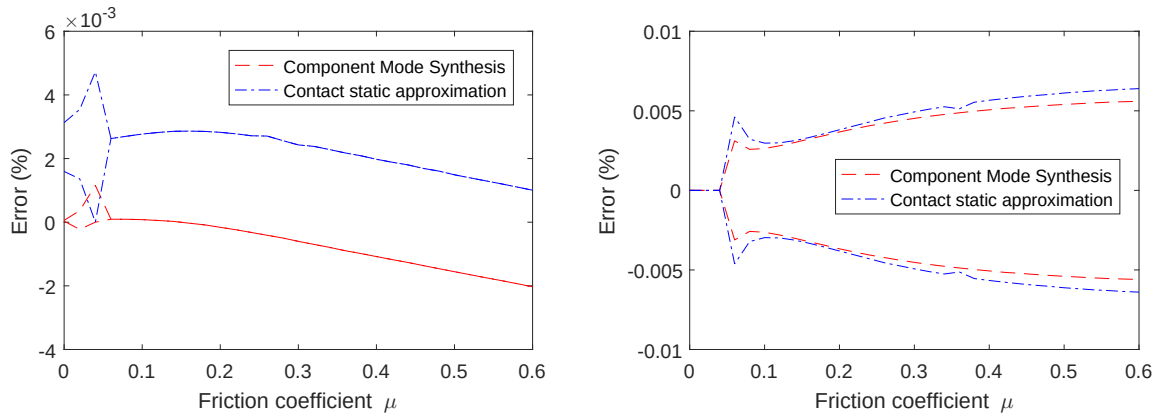

Figure 11: Relative errors of the frequency and absolute errors on the divergence rate of complex modes without damping for $\Delta V_y/V = 1\%$ (a: Frequency, b: Divergence rate)

6.5. Transient results

Transient results corresponding to the unstable case founded in the previous section are determined using a numerical time integration from given initial conditions. In all the following results, the integration starts from the equilibrium i.e. the initial displacements are the displacements obtained from the quasi-static solution and the initial velocities are null. At this point, it is important to recall that the initial conditions can influence the final limit cycle. However, it is especially true in the case of several unstable modes as shown for instance in [22]. When only one mode is unstable as in the present case, it is also true but particularly when initial conditions are

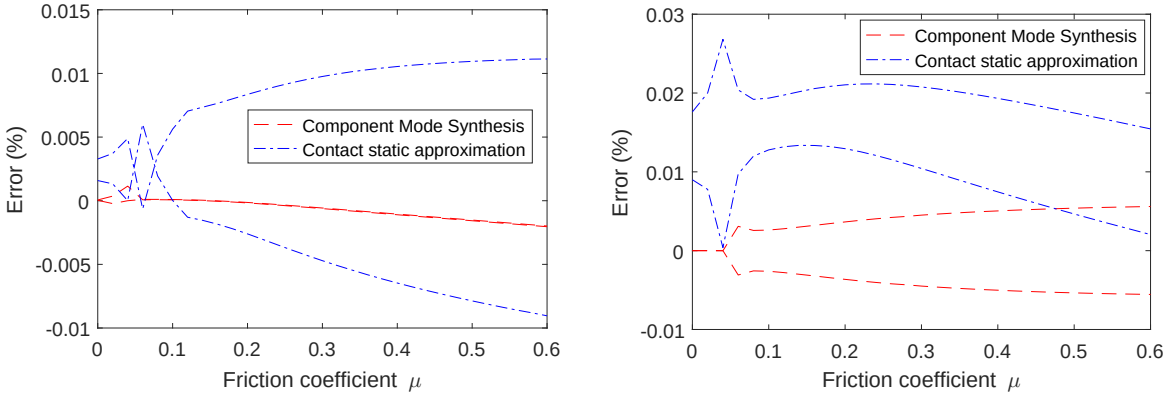

Figure 12: Relative errors of the frequency and absolute errors on the divergence rate of complex modes with damping for $\Delta V_y/V = 1\%$ (a: Frequency, b: Divergence rate)

far from the quasi-static equilibrium. The parameters $V_x = 10$ m/s, $\mu = 0.3$ and $\Delta V_y/V = 1\%$ are used. The time step for the integration is $\Delta t = 1\mu$s. Results obtained with the full non-reduced model are first discussed. Reduced solutions are then presented.

6.5.1. Full model

Figs. 13 and 14 show the time series of the normal and lateral contact resultant forces F_n and F_t. The tangential resultant force increases until a pronounced stick/slip oscillation builds up as shown in Fig. 15. When the tangential contact resultant force is smaller than the traction bound μF_n, a transient stick zone appears at the leading edge of the effective contact region as shown in Fig. 16.

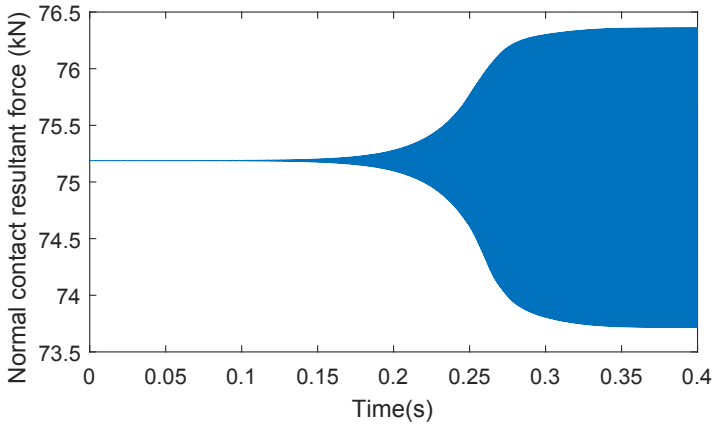

Figure 13: Evolution of the normal contact resultant force

The time series of the lateral velocity of a point outside the contact zone with coordinates (-0.01, 0, -0.01), *i.e.* at 1 cm from the contact zone in the vertical and longitudinal directions, is presented in the Figure 17a. The spectrogram in Fig. 17b allows to observe which frequencies are present in the solution and when they appear. A fundamental frequency is founded at $f_0 = 1612.9$ Hz which gets very close to the frequency of the unstable complex mode provided by stability analysis (1609 Hz). In the steady-state response, harmonic frequencies $f_k = kf_0$ appear. Although in this case, the fundamental frequency is not so different from the frequency of the unstable

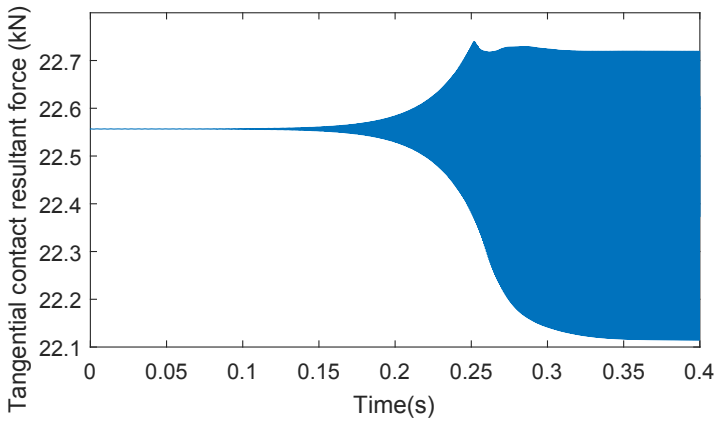

Figure 14: Evolution of the tangential contact resultant force

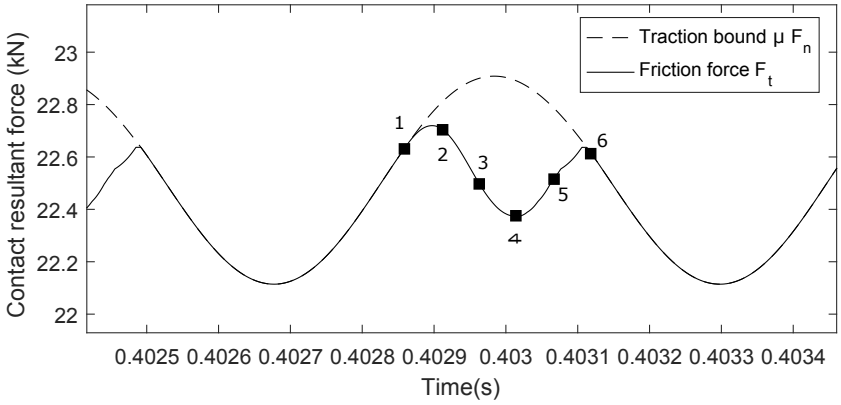

Figure 15: Zoom on time series of the contact resultant forces ; the status of the contact points at the time steps marked with Arabic numerals is represented Fig. 16

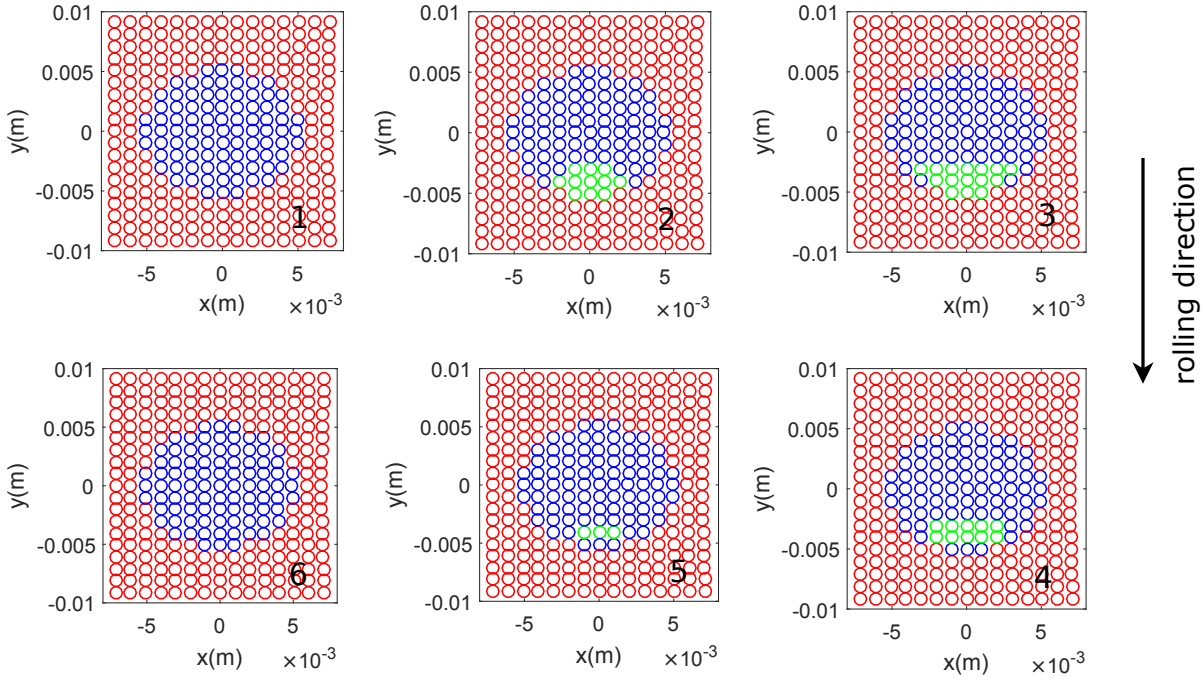

Figure 16: Status of nodes in the potential contact zone: no contact zone (red), slip zone (blue) and stick zone (green). The Arabic notations ”1”, ”2”, ”3”, ”4”, ”5” and ”6” refer to Fig. 15 where the points are equitably distributed over time in the limit cycle

complex mode, these results show the advantages of the nonlinear time integration method compared with the stability analysis. Indeed, the amplitude of the vibrations and the harmonic frequencies cannot be determined by the complex eigenvalue analysis.

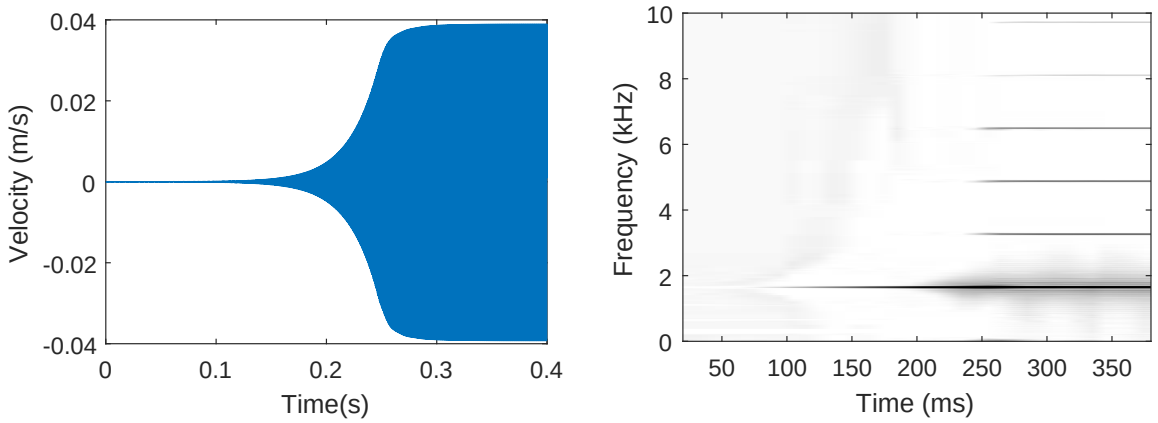

(a) (b)

Figure 17: Tangential velocity of a point outside the contact zone with coordinates (-0.01, 0, -0.01) (a: Temporal evolution, b: Spectrogram (time-frequency))

6.5.2. Reduced models

The two reduction strategies presented in section 3 are tested using 160 free-interface normal modes in the frequency range up to 7510 Hz and 1323 residual attachment modes corresponding to 1323 degrees of freedom on the potential contact interface. For the classical CMS method, a reduced integrator matrix of size 1473×1473 is then obtained while the size of the initial matrix is 239358×239358. This reduced matrix is full but may be factorized before the iterative computation. The problem is therefore reduced significantly. For the contact static approximation, the size of the integrator matrix is reduced to 160×160 which induces a high gain in computation times.

Concerning the precision of the reduced models, the lateral velocity of the point outside the contact zone with coordinates (-0.01, 0, -0.01) obtained with the reduced basis are presented in Figs. 18 and 19 in comparison with the full solution. The fundamental frequencies of the three solutions are very close to each other. With the same initial conditions, the amplitudes of the reduced solutions in the transient response are greater than the full solution. It is well-known that the alteration of the transient evolution of modal participations in the transient state can lead to an acceleration or a deceleration of the transient response [22]. In the present case, the reduced solutions are clearly accelerated, which explains the differences in amplitudes. In the steady-state response (Fig. 19b), the fundamental frequencies obtained with both reduction bases are 1615.5 Hz. The corresponding error (0.16 %) is small. In addition, the amplitude of the three solutions are very similar, with an error of 2.3% on the maximum amplitude. The corresponding spectra are also given in Fig. 20 showing a good agreement between the reduced solutions and the full solution: an error of 0.15 dB at the fundamental frequency and errors of $0.02, 0.73$ and 1.12 dB at the harmonic frequencies.

In addition, it should be noted that the computation times resulting from the use of the reduction bases CMS and CSA are respectively ten and fifteen times shorter than for the computation of the full solution.

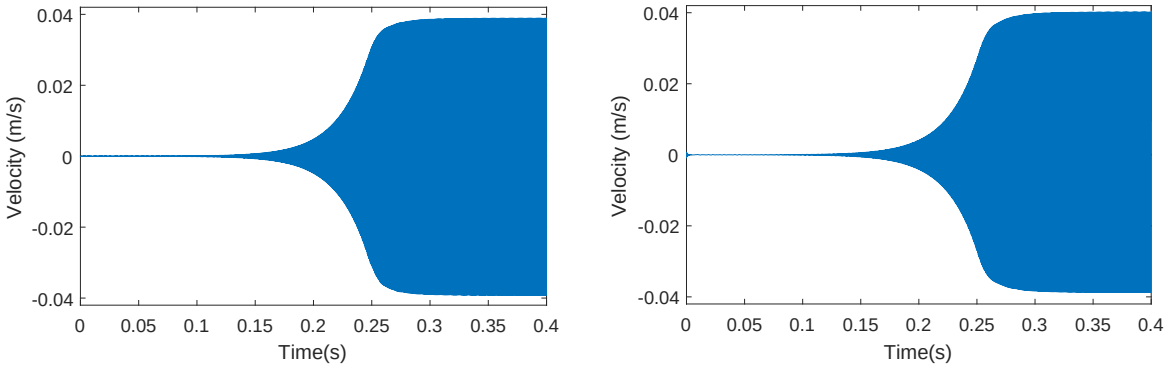

(a) (b)

Figure 18: Lateral velocity in a point outside the contact zone with coordinates (-0.01, 0, -0.01) obtained with the reduced basis (a: Component Mode Synthesis, b: Contact static approximation)

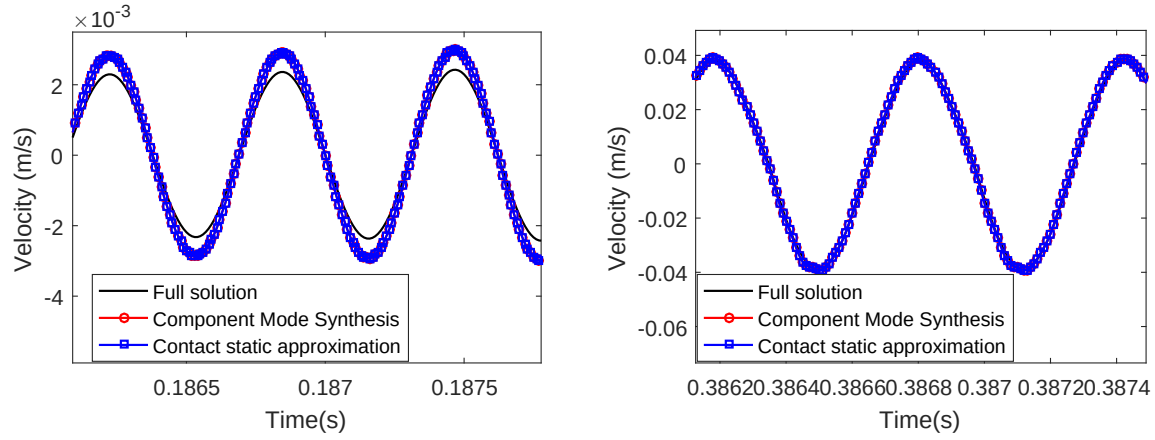

(a) (b)

Figure 19: Zoom on time series of the lateral velocity in a point outside the contact zone with coordinates (-0.01, 0, -0.01) obtained with the reduced basis (a: In the transient response, b: In the steady-state response)

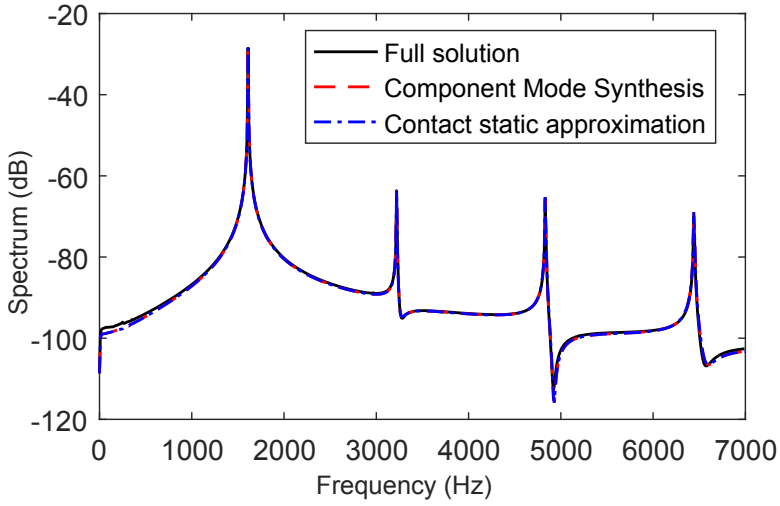

Figure 20: Power spectrum (dB re 1 m/s) of the steady-state lateral velocity in a point outside the contact zone with coordinates (-0.01, 0, -0.01) obtained with the reduced basis

Although the performance of the reduction bases are rather impressive, it is difficult to generalize this result to other cases or applications since it strongly depends on the frequencies involved in the nonlinear solution. In the present case, the nonlinear effects seem to be localized to the contact area, which is coherent with the approximations induced by the two reduction strategies. The amplitude of the harmonics in the velocity spectrum of the point outside the contact zone are quite small compared with the amplitude of the peak at the fundamental frequency. For cases with a greater contribution of harmonics, it might be necessary to complete the basis with normal modes at higher frequencies.

To be complete, it should also be noted here that several non linear methods exist for the direct computation of the steady-state solution, even if they have not been used much in the case of rolling contact systems. In particular, when only one mode is unstable, nonlinear frequency-domain methods like for instance the constrained harmonic balance method (CHBM) proposed by [52] could undoubtedly be an efficient alternative to the time integration method. Other techniques like the shooting method or the orthogonal collocation method could also be used [44, 45, 53]. However, the main objective of the paper does not concern the performance of the time integration scheme but the use of a full finite element approach to study the dynamics of rolling/sliding contact systems at high frequencies, notably in order to calculate reference solutions. Solutions provided by time integrations are often used as reference solutions even when effective nonlinear methods like the CHBM can be used. Moreover, the time integration method has the advantage of providing the transient part of the solution and allows the steady-state solution to be linked with initial conditions. Finally, a third reason for using the time integration method is that it could be used without adaptation for systems exhibiting several unstable modes in the complex eigenvalue analysis, which is not a rare case, for instance in curve squeal problems.

7. Conclusion

In this paper, a method is proposed for the modeling and analysis of the high-frequency friction-induced instabilities of two structures in rolling contact in time and frequency domains. A full finite element formulation around the stationary position in an Eulerian reference frame is derived with a fine discretization of the contact surface combined with unilateral and Coulomb friction laws with constant friction coefficient. Appropriate numerical techniques are used in order to solve the nonlinear discrete equations in quasi-static or dynamic conditions. In addition to the transient approach, a stability analysis performed around the full sliding equilibrium position allows to determine unstable modes and frequencies.

In order to reduce the computational effort, reduction strategies are proposed for both domains. The first technique uses a classical CMS reduced basis including free-interface normal modes and static attachment modes. A second technique consists in simply adding a residual static contact flexibility to the free-interface normal modes when solving the frictional contact equations (contact static approximation). It significantly differs from classical reduction bases used in previous papers and is well suited to this kind of problem where the contact area is small compared to the structures and proves to be efficient in computation cost.

The method is tested in the case of frictional rolling contact between two annular cylinders. The quasi-static results show a good agreement with the ones obtained with Kalker's CONTACT software. In case of full sliding, the stability analysis brings out a mode coupling instability when the contact zone is laterally shifted from the center of the cylinders. In the unstable configuration, the numerical integration provides solutions in the time

domain which are coherent with the stability results. In particular, the unstable frequency determined by this analysis is very close to the fundamental frequency observed in the transient solution. The status of the nodes at the contact zone in the self-sustained vibrations clearly show slip-stick limit cycles.

Concerning the performance of the reduction strategies, the approximate results obtained for the stability analysis show a good agreement with the reference ones. In the time domain, the amplitudes of the reduced solutions are slightly greater than the full solution in the linear phase. However in the steady-state phase, solutions are very similar. This allows to considerably reduce the computational times, especially when the contact static approximation is used.

This methodology may be used later in a large variety of complex friction-mechanical system, especially curve squeal.

Acknowledgements

This work was carried out within the CERVIFER project backed by the ADEME organization and the Haut-de-France region. It was also supported by the LabEx CeLyA of Université of Lyon, operated by the French National Research Agency (ANR-10-LABX-0060/ANR-11-IDEX-0007). The authors gratefully acknowledge the support of these institutions.

References

[1] M. J. Rudd, Wheel/rail noise-part ii: Wheel squeal, Journal of Sound and Vibration 46 (3) (1976) 381–394.

[2] P. J. Remington, Wheel/rail squeal and impact noise: What do we know? what don't we know? where do we go from here?, Journal of Sound and Vibration 116 (2) (1987) 339–353.

[3] N. Vincent, J.-R. Koch, H. Chollet, J.-Y. Guerder, Curve squeal of urban rolling stockpart 1: State of the art and field measurements, Journal of sound and vibration 293 (3) (2006) 691–700.

[4] M. A. Heckl, I. D. Abrahams, Curve squeal of train wheels, part 1: mathematical model for its generation, Journal of Sound and Vibration 229 (3) (2000) 669–693.

[5] M. A. Heckl, Curve squeal of train wheels, part 2: Which wheel modes are prone to squeal?, Journal of Sound and Vibration 229 (3) (2000) 695–707.

[6] C. Glocker, E. Cataldi-Spinola, R. I. Leine, Curve squealing of trains: Measurement, modelling and simulation, Journal of Sound and Vibration 324 (1) (2009) 365–386.

[7] A. Pieringer, A numerical investigation of curve squeal in the case of constant wheel/rail friction, Journal of Sound and Vibration 333 (18) (2014) 4295–4313.

[8] I. Zenzerovic, W. Kropp, A. Pieringer, An engineering time-domain model for curve squeal: Tangential point-contact model and green's functions approach, Journal of Sound and Vibration 376 (2016) 149–165.

[9] B. Ding, G. Squicciarini, D. J. Thompson, Effects of rail dynamics and friction characteristics on curve squeal, in: Journal of Physics: Conference Series, Vol. 744, IOP Publishing, 2016, p. 012146.

[10] B. Ding, G. Squicciarini, D. J. Thompson, R. Corradi, An assessment of mode-coupling and falling-friction mechanisms in railway curve squeal through a simplified approach, Journal of Sound and Vibration 423 (2018) 126–140.

[11] P. Wriggers, T. A. Laursen, Computational contact mechanics, Springer, The Netherlands, 2006.

[12] B. Jacobson, J. J. Kalker, Rolling contact phenomena, Springer, New-York, 2010.

[13] H. Hertz, Über die berührung fester elastischer körper., Journal für die reine und angewandte Mathematik 92 (1882) 156–171.

[14] J. J. Kalker, Wheel-rail rolling contact theory, Wear 144 (1-2) (1991) 243–261.

[15] P. J. Vermeulen, K. L. Johnson, Contact of nonspherical elastic bodies transmitting tangential forces, Journal of Applied Mechanics 31 (2) (1964) 338–340.

[16] Z. Y. Shen, J. K. Hedrick, J. A. Elkins, A comparison of alternative creep force models for rail vehicle dynamic analysis, Vehicle System Dynamics 12 (1-3) (1983) 79–83.

[17] J.-B. Ayasse, H. Chollet, Handbook of railway vehicle dynamic - Chapter 4: Wheel–Rail Contact, CRC Press - Taylor & Francis Group, Boca Raton, FL, 2006.

[18] D. J. Thompson, Railway noise and vibration: mechanisms, modelling and means of control, Elsevier, Oxford, 2008.

[19] J. J. Kalker, A fast algorithm for the simplified theory of rolling contact, Vehicle system dynamics 11 (1) (1982) 1–13.

[20] J.-J. Sinou, L. Jezequel, Mode coupling instability in friction-induced vibrations and its dependency on system parameters including damping, European Journal of Mechanics-A/Solids 26 (1) (2007) 106–122.

[21] L. Charroyer, O. Chiello, J.-J. Sinou, Parametric study of the mode coupling instability for a simple system with planar or rectilinear friction, Journal of Sound and Vibration 384 (2016) 94–112.

[22] A. Loyer, J.-J. Sinou, O. Chiello, X. Lorang, Study of nonlinear behaviors and modal reductions for friction destabilized systems. application to an elastic layer, Journal of Sound and Vibration 331 (5) (2012) 1011–1041.

[23] S. Bogdanski, M. Olzak, J. Stupnicki, Numerical stress analysis of rail rolling contact fatigue cracks, Wear 191 (1-2) (1996) 14–24.

[24] M. Wiest, E. Kassa, W. Daves, J. C. Nielsen, H. Ossberger, Assessment of methods for calculating contact pressure in wheel-rail/switch contact, Wear 265 (9-10) (2008) 1439–1445.

[25] M. Toumi, H. Chollet, H. Yin, Finite element analysis of the frictional wheel-rail rolling contact using explicit and implicit methods, Wear 366 (2016) 157–166.

[26] X. Zhao, Z. Li, The solution of frictional wheel–rail rolling contact with a 3d transient finite element model: Validation and error analysis, Wear 271 (1-2) (2011) 444–452.

[27] C. J. M. Van Ruiten, Mechanism of squeal noise generated by trams, Journal of Sound and Vibration 120 (2) (1988) 245–253.

[28] F. G. De Beer, M. H. A. Janssens, P. P. Kooijman, Squeal noise of rail-bound vehicles influenced by lateral contact position, Journal of Sound and Vibration 267 (3) (2003) 497–507.

[29] G. Xie, P. Allen, S. D. Iwnicki, A. Alonso, D. J. Thompson, C. J. C. Jones, Z. Y. Huang, Introduction of falling friction coefficients into curving calculations for studying curve squeal noise, Vehicle system dynamics 44 (sup1) (2006) 261–271.

[30] G. Squicciarini, S. Usberti, D. J. Thompson, R. Corradi, A. Barbera, Curve squeal in the presence of two wheel/rail contact points, in: Noise and Vibration Mitigation for Rail Transportation Systems, Proceedings of the 11th International Workshop on Railway Noise, Uddevalla, Sweden, 9-13 September 2013, Vol. 126 of Notes on Numerical Fluid Mechanics and Multidisciplinary Design, Springer, 2015, pp. 603–610.

[31] U. Fingberg, A model of wheel-rail squealing noise, Journal of Sound and Vibration 143 (3) (1990) 365–377.

[32] F. J. Périard, Wheel-rail noise generation: curve squealing by trams, TU Delft, Delft University of Technology, 1998.

[33] O. Chiello, J.-B. Ayasse, N. Vincent, J.-R. Koch, Curve squeal of urban rolling stock - part 3: Theoretical model, Journal of sound and vibration 293 (3) (2006) 710–727.

[34] Z. Y. Huang, D. J. Thompson, C. J. C. Jones, Squeal prediction for a bogied vehicle in a curve, in: Noise and Vibration Mitigation for Rail Transportation Systems, Proceedings of the 9th International Workshop on Railway Noise, Munich, Germany, 4-8 September 2007, Vol. 99 of Notes on Numerical Fluid Mechanics and Multidisciplinary Design, Springer, 2008, pp. 313–319.

[35] J.-F. Brunel, P. Dufrénoy, M. Naït, J.-L. Muñoz, F. Demilly, Transient models for curve squeal noise, Journal of sound and vibration 293 (3) (2006) 758–765.

[36] J.-J. Sinou, Transient non-linear dynamic analysis of automotive disc brake squeal–on the need to consider both stability and non-linear analysis, Mechanics Research Communications 37 (1) (2010) 96–105.

[37] K. L. Johnson, Contact mechanics, Cambridge university press, Cambridge, 1987.

[38] M. Jean, The non-smooth contact dynamics method, Computer methods in applied mechanics and engineering 177 (3) (1999) 235–257.

[39] P. Chambrette, L. Jezequel, Stability of a beam rubbed against a rotating disc, European journal of mechanics. A. Solids 11 (1) (1992) 107–138.

[40] M. Raous, S. Barbarin, D. Vola, Numerical characterization and computation of dynamic instabilities for frictional contact problems, in: Friction and Instabilities, Udine UD, Italie, Springer, 2002, pp. 233–291.

[41] A. D. Kudawoo, Problèmes industriels de grande dimension en mécanique numérique du contact: performance, fiabilité et robustesse., Ph.D. thesis, Aix-Marseille (2012).

[42] D. Brizard, O. Chiello, J.-J. Sinou, X. Lorang, Performances of some reduced bases for the stability analysis of a disc/pads system in sliding contact, Journal of Sound and Vibration 330 (4) (2011) 703–720.

[43] X. Lorang, O. Chiello, Stability and transient analysis in the modelling of railway disc brake squeal, in: Noise and Vibration Mitigation for Rail Transportation Systems, Proceedings of the 9th International Workshop on Railway Noise, Munich, Germany, 4-8 September 2007, Vol. 99 of Notes on Numerical Fluid Mechanics and Multidisciplinary Design, Springer, 2008, pp. 447–453.

[44] A. Steindl, H. Troger, Methods for dimension reduction and their application in nonlinear dynamics, International Journal of Solids and Structures 38 (10) (2001) 2131–2147.

[45] G. Kerschen, M. Peeters, J.-C. Golinval, A. F. Vakakis, Nonlinear normal modes, part i: A useful framework for the structural dynamicist, Mechanical Systems and Signal Processing 23 (1) (2009) 170–194.

[46] X. Lorang, F. Foy-Margiocchi, Q. S. Nguyen, P.-E. Gautier, Tgv disc brake squeal, Journal of Sound and Vibration 293 (3-5) (2006) 735–746.

[47] R. R. Craig, C. J. Chang, On the use of attachment modes in substructure coupling for dynamic analysis, Proc. AIAA/ASME 18th Structures, Structural Dynamics, and Materials Conf. (1977) 89–99.

[48] R. R. Craig, A review of time-domain and frequency-domain component mode synthesis method, Combined Experimental/Analytical Modeling of Dynamic Structural Systems (3rd Edition) 67 (1985) 1–30.

[49] H. B. Khenous, J. Pommier, Y. Renard, Hybrid discretization of the signorini problem with coulomb friction. theoretical aspects and comparison of some numerical solvers, Applied Numerical Mathematics 56 (2) (2006) 163–192.

[50] N. Hoffmann, L. Gaul, Effects of damping on mode-coupling instability in friction induced oscillations, ZAMM-Journal of Applied Mathematics and Mechanics/Zeitschrift für Angewandte Mathematik und Mechanik: Applied Mathematics and Mechanics 83 (8) (2003) 524–534.

[51] G. Fritz, J.-J. Sinou, J.-M. Duffal, L. Jézéquel, Investigation of the relationship between damping and mode-coupling patterns in case of brake squeal, Journal of Sound and Vibration 307 (3) (2007) 591–609.

[52] N. Coudeyras, J.-J. Sinou, S. Nacivet, A new treatment for predicting the self-excited vibrations of nonlinear systems with frictional interfaces: The constrained harmonic balance method, with application to disc brake squeal, Journal of sound and vibration 319 (3-5) (2009) 1175–1199.

[53] L. Charroyer, O. Chiello, J.-J. Sinou, Self-excited vibrations of a non-smooth contact dynamical system with planar friction based on the shooting method, International Journal of Mechanical Sciences 144 (2018) 90–101.